(C.B.); and by NIH grant HG003224 (F.P.R.). I.L. is a postdoctoral fellow with the Fonds Wetenschappelijk Onderzoek–Vlanderen. M.V. is a "Chercheur Qualifié Honoraire" from the Fonds de la Recherche Scientifique (FRS-FNRS, French Community of Belgium). We thank members of our laboratories for helpful discussions and Agencourt Biosciences for sequencing assistance. All data sets can be downloaded from our Web site (http://interactome.dfci.harvard.edu/S_cerevisiae).

Supporting Online Material
www.sciencemag.org/cgi/content/full/1158684/DC1
SOM Text
Figs. S1 to S35
Tables S1 to S5
References

4 April 2008; accepted 1 August 2008
Published online 21 August 2008;
10.1126/science.1158684
Include this information when citing this paper.

Ceramide Biogenesis Is Required for Radiation-Induced Apoptosis in the Germ Line of *C. elegans*

Xinzhu Deng,[1] Xianglei Yin,[1] Richard Allan,[1] Diane D. Lu,[1] Carine W. Maurer,[2] Adriana Haimovitz-Friedman,[3] Zvi Fuks,[3] Shai Shaham,[2] Richard Kolesnick[1]*

Ceramide engagement in apoptotic pathways has been a topic of controversy. To address this controversy, we tested *loss-of-function (lf)* mutants of conserved genes of sphingolipid metabolism in *Caenorhabditis elegans*. Although somatic (developmental) apoptosis was unaffected, ionizing radiation–induced apoptosis of germ cells was obliterated upon inactivation of ceramide synthase and restored upon microinjection of long-chain natural ceramide. Radiation-induced increase in the concentration of ceramide localized to mitochondria and was required for BH3-domain protein EGL-1–mediated displacement of CED-4 (an APAF-1–like protein) from the CED-9 (a Bcl-2 family member)/CED-4 complex, an obligate step in activation of the CED-3 caspase. These studies define CEP-1 (the worm homolog of the tumor suppressor p53)–mediated accumulation of EGL-1 and ceramide synthase–mediated generation of ceramide through parallel pathways that integrate at mitochondrial membranes to regulate stress-induced apoptosis.

Although studies that use genetic deficiency in ceramide production support it as essential for apoptosis in diverse models (*1*), many have questioned whether ceramide functions as a bona fide transducer of apoptotic signals (*2*). One reason for skepticism is that, despite delineation of a number of ceramide-activated proteins, no single protein has been identified as mediator of ceramide-induced apoptosis. Recent studies have suggested an alternate mode of ceramide action, based on its capacity to self-associate and locally rearrange membrane bilayers into ceramide-rich macrodomains (1 to 5 μm in diameter), which are sites of protein concentration and oligomerization (*3*). Ceramide may thus mediate apoptosis through its ability to reconfigure membranes, coordinating protein complexation at critical junctures of signaling cascades.

To establish the role of ceramide definitively, we used a model of radiation-induced apoptosis in *Caenorhabditis elegans* germ cells (*4*). Germline stem cells, located at the distal gonad tip, divide incessantly throughout adult life, with daughter cells arresting in meiotic prophase. Upon exiting prophase, germ cells become sensitive to radiation-induced apoptosis, detected morphologically just proximal to the bend of the gonadal arm (*5*). This apoptotic pathway is antagonized by the ABL-1 tyrosine kinase, requiring sequentially the cell cycle checkpoint genes *rad-5*, *hus-1*, and *mrt-2*; the *C. elegans* p53 homolog *cep-1*; and the genes making up the conserved apoptotic machinery, the caspase *ced-3*, the apoptotic protease activating factor 1–like protein *ced-4*, the Bcl-2 protein *ced-9*, and the BH3-domain protein *egl-1*. This pathway differs from apoptotic somatic cell death, which is not subject to upstream checkpoint regulation via the CEP-1 pathway (*5*, *6*).

We identified conserved genes that regulate *C. elegans* sphingolipid intermediary metabolism and tested deletion alleles (Table 1 and table S1). Screening for mutants resistant to radiation-induced germ cell apoptosis revealed apoptosis suppression in only deletion mutants of *hyl-1* and *lagr-1*, two of the three ceramide synthase (CS) genes (Fig. 1A). CS gene products regulate de novo ceramide biosynthesis, acylating sphinganine to form dihydroceramide that is subsequently converted to ceramide by a desaturase (*7*). CSs contain six to seven putative transmembrane domains and a Lag1p motif [which confers enzyme activity (*8*)], regions conserved in the *C. elegans* orthologs. The deleted CS sequences in *hyl-1(ok976)* and *lagr-1(gk327)* result in frameshifts that disrupt the Lag1p motifs (fig. S1A). We detected a ~1.6-kb *hyl-1* transcript in wild-type (WT) worms and a smaller ~1.35-kb transcript in *hyl-1(ok976)*, whereas we observed a ~1.4-kb *lagr-1* transcript in WT worms and a ~1.25-kb transcript in *lagr-1(gk327)* (fig. S1B). In contrast, a deletion mutant of the third *C. elegans* CS (*9*, *10*), *hyl-2(ok1766)*, lacking a 1626-base pair fragment of the *hyl-2* gene locus that eliminates exons 2 to 5 corresponding to 74% of the coding sequence, displayed no defect in germ cell death (fig. S1C).

In N2 WT strain young adults, apoptotic germ cells gradually increased in abundance with age from a baseline of 0.7 ± 0.1 to 1.8 ± 0.2 corpses per distal gonad arm over 48 hours. Exposure to a 120-gray (Gy) ionizing radiation dose increased germ cell apoptosis to 5.2 ± 0.3 cells 36 to 48 hours after treatment. In contrast, in *hyl-1 (ok976)* and *lagr-1(gk327)* animals, age-dependent and radiation-induced germ cell apoptosis were nearly abolished (Fig. 1A). Similar effects were observed in the *lagr-1(gk327);hyl-1(ok976)* double mutant (Fig. 1B). The rate of germ cell corpse removal was unaffected in CS mutants, excluding the possibility that defective corpse engulfment elevated corpse numbers (table S2). In contrast, *loss-of-function (lf)* mutations of *hyl-1* or *lagr-1* did not affect developmental somatic cell death, nor did the *lf hyl-2(ok1766)* mutation (table S3). These studies indicate a requirement for two *C. elegans* CS genes for radiation-induced germline apoptosis.

To confirm ceramide as critical for germline apoptosis, we injected C_{16}-ceramide into gonads of young adult WT worms. C_{16}-ceramide is the predominant ceramide species in apoptosis induction by diverse stresses in multiple organisms (*11*) and in low abundance in *C. elegans* (*12*, *13*). C_{16}-ceramide microinjection resulted in time- and dose-dependent increases in germ cell apoptosis (Fig. 1C), with a median effective dose of ~0.05 μM gonadal ceramide. Peak effect occurred at ~0.1 μM gonadal ceramide at 36 hours (6.6 ± 0.8 versus 1.5 ± 0.4 cell corpses per distal gonad arm, $P < 0.0001$), qualitatively and quantitatively mimicking the 120-Gy effect in WT worms. In contrast, C_{16}-dihydroceramide, which differs from C_{16}-ceramide in a trans double bond at sphingoid base position four to five, was without effect (0.71 ± 0.28 cell corpses per distal gonad arm at ~1 μM), indicating specificity for ceramide in apoptosis induction. Furthermore, C_{16}-ceramide microinjection into *lagr-1(gk327);hyl-1(ok976)* animals (~1 μM gonadal ceramide) resulted in a 5.7-fold increase in germ cell apoptosis (from 0.60 ± 0.17 to 3.43 ± 0.88, $P <$ 0.0001) (Fig. 1D). Note that the baseline level of apoptosis in *lagr-1(gk327);hyl-1(ok976)* was less than one-half that in WT worms. Moreover, ~0.005 μM gonadal ceramide, a concentration without impact on germ cell apoptosis, completely restored radiation (120 Gy)–induced apoptosis, an effect inhibitable in a *lf ced-3* background (Fig. 1E). C_{16}-ceramide's ability to bypass the genetic defect and restore the radiation-response pheno-

[1]Laboratory of Signal Transduction, Memorial Sloan-Kettering Cancer Center (MSKCC), New York, NY 10021, USA. [2]Laboratory of Developmental Genetics, Rockefeller University, New York, NY, 10021, USA. [3]Department of Radiation Oncology, Memorial Sloan-Kettering Cancer Center, New York, NY 10021, USA.

*To whom correspondence should be addressed. E-mail: r-kolesnick@ski.mskcc.org

type is strong evidence that *hyl-1* and *lagr-1* represent legitimate *C. elegans* CS genes. Animals with *sphk-1(ok1097)*, a null allele of sphingosine kinase (SPHK), which prevents conversion of ceramide to its anti-apoptotic derivative sphingosine 1-phosphate (S1P) (*14*), displayed high baseline germ cell death and were hypersensitive to radiation-induced germ cell apoptosis (fig. S2, A and B), inhibitable (by 85 ± 9%) in a *lagr-1(gk327);sphk-1(ok1097)* double mutant. Collectively, these studies identify ceramide as a critical effector of radiation-induced germ cell apoptosis, although they do not define its mode of engaging the apoptotic pathway.

Inactivation of the *C. elegans* ABL-1 ortholog in the *lf* mutant *abl-1(ok171)* (or by RNA interference) increases baseline and post-radiation germ cell apoptosis, modeling radiation hypersensitivity

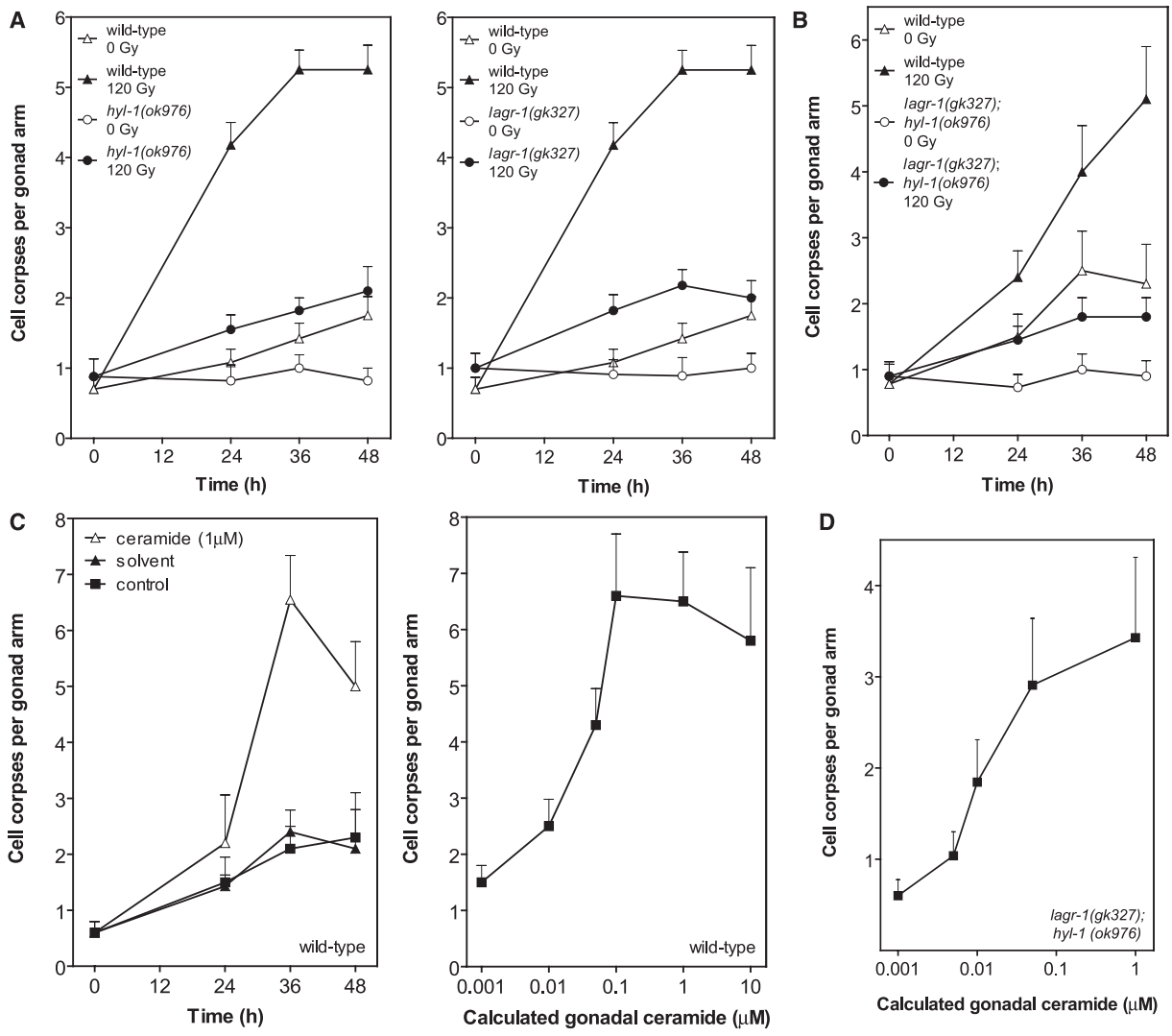

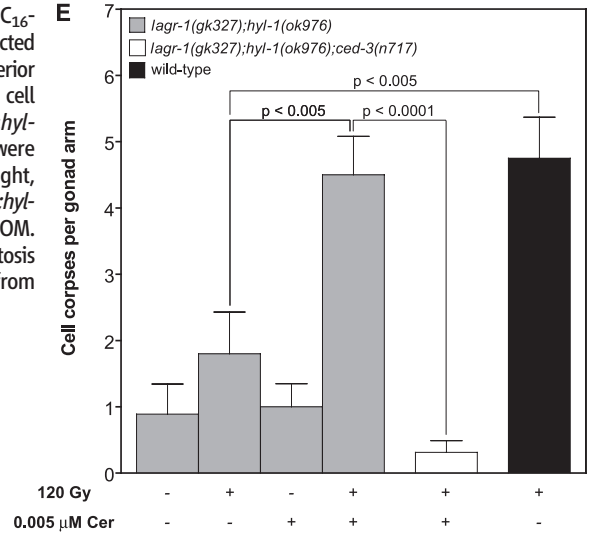

Fig. 1. *lf hyl-1* and *lagr-1* prevent radiation-induced germ cell apoptosis, reversible by C_{16}-ceramide. WT and mutant worms were synchronized at 20°C and irradiated (**A**, **B**, and **E**) or injected with C_{16}-ceramide into the posterior gonad (**C** to **E**) at 24 hours after the L4 stage. The posterior gonad distal arm was scored for cell corpses under Nomarski optics. Time dependence of germ cell corpse induction in *hyl-1(ok976)* (left) and *lagr-1(gk327)* (right) (A) and in *lagr-1(gk327);hyl-1(ok976)* (B) after 120 Gy is shown. WT data are identical in (A), left and right; these panels were separated for clarity. C_{16}-ceramide microinjection induces time- (left) and dose-dependent (right, at 36 hours) germ cell apoptosis in WT worms (C) and dose-dependent apoptosis in *lagr-1(gk327);hyl-1(ok976)* at 36 hours (D). Gonadal ceramide concentration was calculated as described in the SOM. (E) Sublethal C_{16}-ceramide microinjection restores radiation (120 Gy)-induced germ cell apoptosis to *lagr-1(gk327);hyl-1(ok976)*. Data (mean ± SEM, represented by error bars) are collated from ≥15 worms per group in (A) to (E).

phenotypes (*15*). To order CS action relative to ABL-1, we generated *hyl-1(ok976);abl-1(ok171)* and *lagr-1(gk327);abl-1(ok171)* and a triple mutant *lagr-1(gk327);hyl-1(ok976);abl-1(ok171)*. *lf hyl-1* or *lagr-1* in an *abl-1(ok171)* genetic background prevented the time-dependent increase in physiologic germ cell apoptosis and completely blocked radiation-induced apoptosis (Fig. 2A, left). Similarly, *lagr-1(gk327);hyl-1(ok976);abl-1(ok171)* displayed inhibition of baseline and radiation-induced germ cell apoptosis (Fig. 2A, right). Thus, increased germ cell apoptosis in irradiated *abl-1(ok171)* depends on the CS genes *hyl-1* and *lagr-1*.

In *C. elegans*, DNA damage activates the p53 homolog CEP-1, which is required for transcriptional up-regulation of the BH3-only proteins, EGL-1 and CED-13, that in turn activate the core apoptotic machinery (CED-9, CED-4, and CED-3) (*6*, *16*). Exposure of *hyl-1(ok976)* and *lagr-1 (gk327)* to 120 Gy increased *egl-1* transcripts

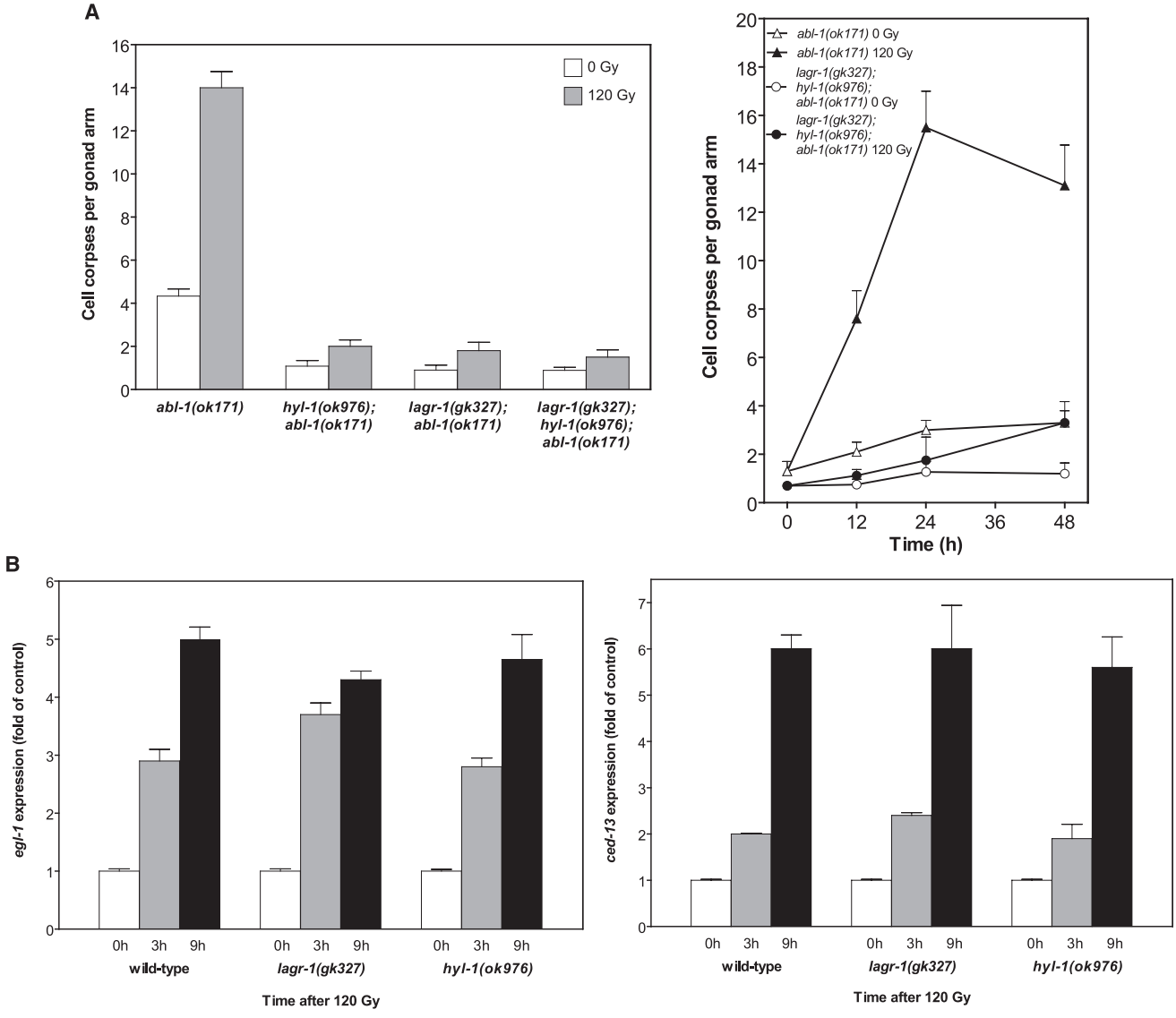

Fig. 2. Role of ceramide in CEP-1/p53–mediated germ cell apoptosis. (**A**) *hyl-1* and *lagr-1* are epistatic to *abl-1* in germ cell apoptosis. Germ cell apoptosis was scored in *abl-1(ok171), hyl-1(ok976);abl-1(ok171), lagr-1(gk327);abl-1(ok171)*, and *lagr-1(gk327);hyl-1(ok976);abl-1(ok171)* at 36 hours (left) and in *lagr-1(gk327);hyl-1(ok976);abl-1(ok171)* at the indicated times after exposure to 120 Gy (right). Data (mean ± SEM, represented by error bars) are collated from 10 to 15 worms per group. (**B**) *hyl-1* and *lagr-1* deletions do not affect 120-Gy–induced p53-mediated *egl-1* (left) and *ced-13* (right) up-regulation measured by reverse transcription polymerase chain reaction. Data (mean ± SEM) are compiled from three experiments. (**C**) Baseline EGL-1 is required for C_{16}-ceramide (~1 μM gonadal ceramide)–induced germ cell apoptosis. Studies were performed as in Fig. 1B. Data (mean ± SEM) are collated from ≥15 worms per group.

four- to fivefold at 9 hours after irradiation (Fig. 2B, left), whereas *ced-13* expression was enhanced five- to sixfold (Fig. 2B, right)—levels comparable to those detected in irradiated WT worms. Thus, the loss of CS did not affect CEP-1 activation upon irradiation, suggesting that ceramide and CEP-1 might function in parallel, coordinately conferring radiation-induced germ cell death.

We reasoned that in contrast to radiation-induced germ cell apoptosis, which apparently requires increased abundance of both BH3-only proteins and ceramide, C_{16}-ceramide provided exogenously might act independent of p53-mediated *egl-1* expression by maximizing the effect of baseline EGL-1. In fact, microinjected C_{16}-ceramide partially restored germ cell death in *cep-1(gk138)* from 0.4 ± 0.13 to 2.5 ± 0.32 corpses per distal gonad arm (Fig. 2C) ($P < 0.001$). As C_{16}-ceramide

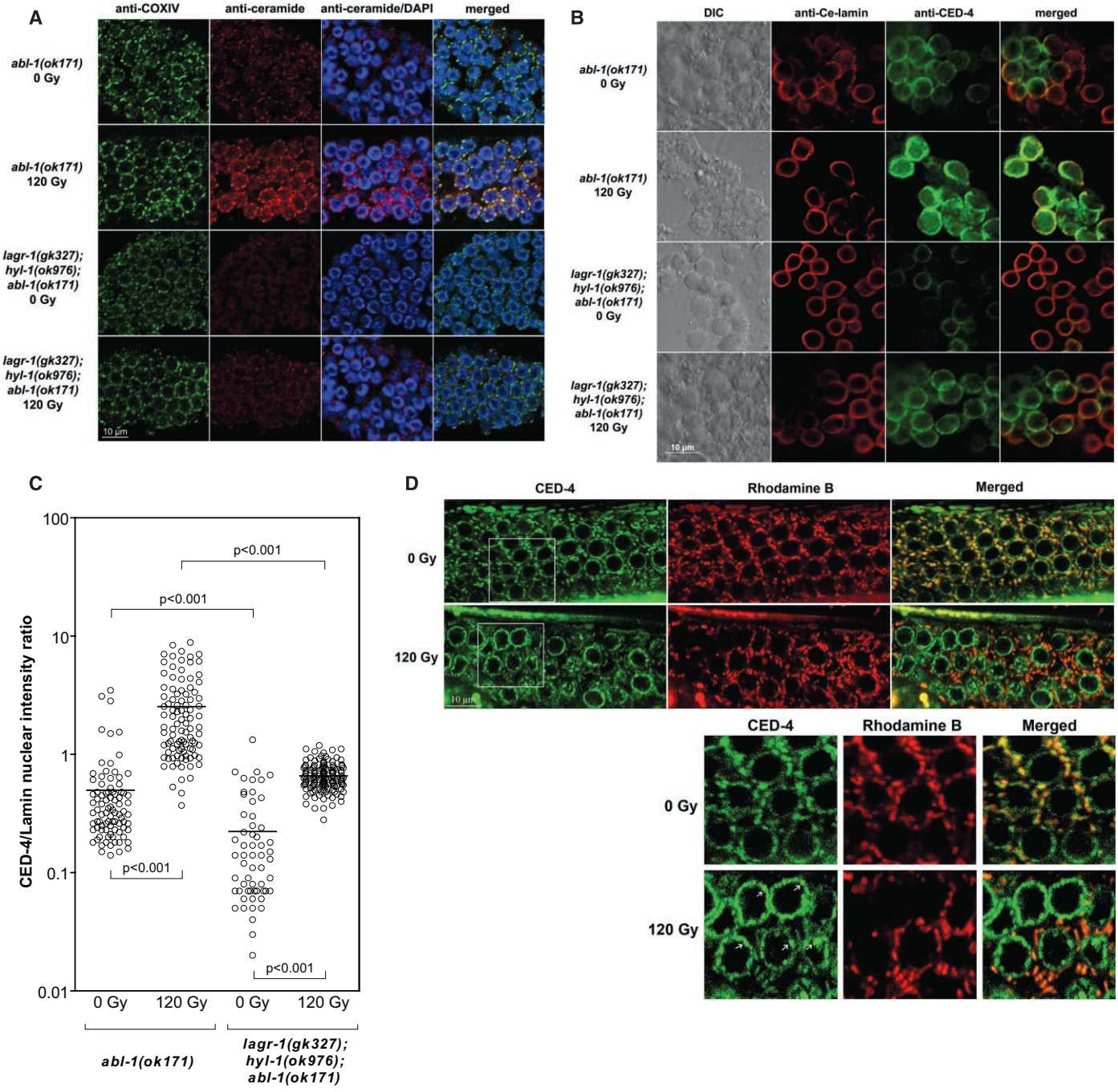

Fig. 3. Mitochondrial ceramide mediates CED-4 displacement. (**A**) Gonads were dissected from young adult *abl-1(ok171)* and *lagr-1(gk327);hyl-1(ok976);abl-1(ok171)* at 24 hours after 120 Gy and stained with anti–COX-IV antibody (green), anti-ceramide antibody (red), and 4′,6′-diamidino-2-phenylindole (blue). (**B** and **C**) Germ cells were released from gonads of young adult *abl-1(ok171)* and *lagr-1(gk327);hyl-1(ok976);abl-1(ok171)* at 24 hours after 120 Gy and stained with anti–Ce-lamin (red) and anti–CED-4 (green). CED-4/lamin intensity in individual germ cell nuclei (circles) was measured using Metamorph software. Horizontal bars indicate means from ≥50 nuclei per group. In *lagr-1(gk327);hyl-1(ok976);abl-1(ok171)*, the baseline CED-4/lamin ratio is reduced by 63%, and the post-radiation fold and absolute change are reduced by 40% and 78%, respectively, as compared with *abl-1(ok171)* animals. (**D**) L1 larvae of *opls219*, cultured in Rhodamine B–containing plates until the young adult stage, were exposed to 120 Gy, and GFP (CED-4) and Rhodamine B (mitochondria) signals were imaged at 36 hours post-irradiation. Images represent single confocal planes from the distal gonad of *opls219* (upper panels). Boxed insets (lower panels) were enlarged 1.75 times to ease the observation of colocalized CED-4/Rhodamine B mitochondrial yellow signal (top right bottom panel) pre-irradiation and green nuclear CED-4 platformlike structures post-irradiation (white arrows in bottom left lower panel).

Table 1. Role of *C. elegans* orthologs of sphingolipid metabolism in radiation-induced apoptosis. The family of sphingolipids and associated metabolic enzymes involved in ceramide intermediary metabolism, conserved from yeast to humans is shown on at left. Thick arrows designate the de novo ceramide synthetic pathway. Enzymes listed in bold indicate *C. elegans* enzymes for which *lf* alleles were screened for germ cell apoptosis at 36 hours post–120 Gy (shown at right). Apoptosis inhibition (+) was interpreted relative to WT-irradiated controls. Asterisks indicate hypersensitivity to radiation-induced apoptosis. At least 20 worms were counted per allele. SPT, serine palmitoyltransferase; 3-KSR, 3-ketosphinganine reductase; CerS, ceramide synthase; DES, dihydoceramide desaturase; CerK, ceramide kinase; SMase, sphingomyelinase; CDase, ceramidase; SphK, sphingosine kinase; S1PPL, S1P lyase.

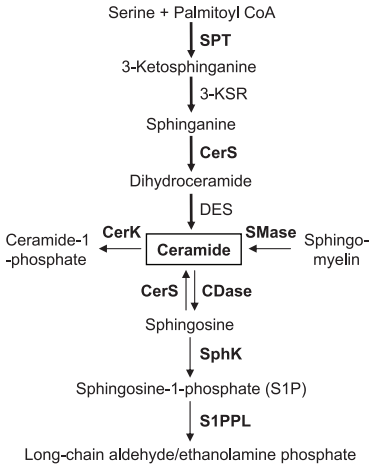

Mammalian gene product	*C. elegans* orthologous gene(s)	Sequence name	Alleles	Apoptosis inhibition
SPT 1	*sptl-1*	C23H3.4	*ok1693*	–
SPT 2	*sptl-3*	T22G5.5	*ok1927*	–
CerS	*hyl-1*	C09G4.1	*ok976*	+
	hyl-2	K02G10.6	*ok1766*	–
	lagr-1	Y6B3B.10	*gk327* *gk331*	+ +
Acid CDase		F27E5.1	*ok564*	–
SphK-1	*ok1097*	C34C6.5a,b	*ok1097*	–*
S1PPL 1	*tag-38*	B0222.4	*tm470*	–
CerK		T10B11.2	*ok1252*	–
Acid SMase	*asm-1*	B0252.2	*kk-1*	–
	asm-2	ZK455.4	*ok183*	–
	asm-3	W03G1.7a,b	*tm2384*	–
Neutral SMase		T27F6.6	*tm2178*	–

is inactive in the *lf egl-1* mutant *egl-1(n1084n3082)* (Fig. 2C), it appears that there is a requirement for at least a baseline level of BH3-only proteins for ceramide-induced apoptosis. Consistent with this notion, C_{16}-ceramide administration did not increase *egl-1* and *ced-13* transcription (1.2 ± 0.1– and 0.8 ± 0.1–fold of control, respectively, at 5 hours). Furthermore, inactivating the core apoptotic machinery in *lf ced-3(n717)* and *ced-4(n1162)* or in gain-of-function *ced-9(n1950)* animals, which abolish radiation-induced germline apoptosis, similarly abolished C_{16}-ceramide-induced death (Fig. 2C). Collectively, these data indicate that ceramide acts in conjunction with BH3-only proteins upstream of the mitochondrial commitment step of apoptosis in the *C. elegans* germ line.

As these studies point to a mitochondrial site of ceramide action, we devised an immune histochemical approach to evaluate whether ceramide might increase in the mitochondria of *C. elegans* germ cells. We took advantage of the increased frequency of germ cell apoptosis in *abl-1(ok171)*, anticipating a maximized ceramide signal upon irradiation in this strain. Gonads from unirradiated or irradiated worms were dissected, opened by freeze-cracking (*17*), and then stained with MID15B4, a specific anti-ceramide antibody [see the supporting online material (SOM)]. Mitochondria were localized with an antibody to the mitochondrial marker protein OxPhos Complex IV subunit I (COX-IV) or by Rhodamine B staining (*18*). COX-IV staining (green) before and after irradiation displayed a prominent perinuclear distribution reminiscent of mitochondrial topography in some mammalian cell systems (Fig. 3A) (*19*, *20*). Ceramide staining (red) displayed a similar profile and at baseline was faint, increasing 2.4-fold at 24 hours post-irradiation (Fig. 3A and fig. S3) ($P < 0.0001$). Merging the two signals (red and green) revealed that ceramide accumulation was distinctively mitochondrial (yellow). Radiation-induced ceramide accumulation was abrogated in *lagr1(gk327);hyl-1(ok976);abl-1(ok171)* animals (Fig. 3A). Similarly, ceramide increase was abrogated in irradiated *lagr-1(gk327);hyl-1(ok976)* as compared with WT animals (1.2- versus 3.9-fold of unirradiated controls, respectively). These results define ionizing radiation-induced ceramide accumulation in the *C. elegans* germ line as mitochondrial in origin, mediated via the classic ceramide biosynthetic pathway.

We examined whether mitochondrial ceramide accumulation was required for CED-4 redistribution to nuclear membranes. In nonapoptotic somatic cells, CED-4 is sequestered to mitochondria by binding CED-9. When displaced by EGL-1, CED-4 targets nuclear membranes and activates caspase CED-3, necessary for the effector phase of apoptosis (*21*–*24*). For these studies, *abl-1(ok171)* and *lagr-1(gk327);hyl-1(ok976);abl-1(ok171)* animals were exposed to 120 Gy, and germ cells were released from gonads and stained with antibodies against *C. elegans* CED-4 and Ce-lamin, a nuclear membrane marker. CED-4 and Ce-lamin colocalization by confocal microscopy (yellow merged signal) served as readout for nuclear CED-4 redistribution. After irradiation nuclear CED-4 staining intensity increased 4.3-fold from 0.59 ± 0.03 to 2.53 ± 0.42 arbitrary fluorescence units in *abl-1(ok171)* (Fig. 3, B and C) ($P < 0.001$). Consistent with reduced germ cell apoptosis (Fig. 2A), nuclear CED-4 staining is significantly reduced in *lagr-1(gk327);hyl-1(ok976);abl-1(ok171)* (Fig. 3, B and C) [$P <$ 0.001 versus *abl-1(ok171)*]. Specifically, baseline CED-4 intensity at the nuclear membrane is lower in *lagr-1(gk327);hyl-1(ok976);abl-1(ok171)* than in *abl-1(ok171)*, increasing post-irradiation only to the control level of unirradiated *abl-1(ok171)* worms (Fig. 3C), an effect probably of biologic relevance as the biophysical effects of ceramide on membrane structure are concentration-dependent (*1*, *3*).

We also used *opls219* worms, a strain expressing a CED-4::GFP fusion protein (where GFP is green fluorescent protein), which permits in vivo detection of CED-4 trafficking (*25*). *opls219* worms were cultured on plates containing Rhodamine B to stain mitochondria (red). Merged images detect mitochondrial CED-4 as a yellow signal (red and green overlay), whereas nonmitochondrial CED-4 appears green. Although a low-intensity green CED-4 signal was detected in nuclear membranes of unirradiated germ cells, the large majority of CED-4 was present in mitochondria before irradiation. At 36 hours postradiation, the CED-4 signal was markedly reduced in mitochondria, relocalizing primarily to nuclear membranes as bright green platform-like structures (arrows in lower left panel in bottom of Fig. 3D). In eight worms, overall reduction in CED-4 mitochondrial colocalization upon irradiation was ~50% ($P < 0.0001$), abrogated in *lagr-1(gk327);opls219* (fig. S4). Consistent with the anti–CED-4 antibody staining (Fig. 3B), the loss of mitochondrial CED-4 signal in *opls219* was accompanied by a twofold increase in nuclear CED-4 signal, blocked entirely in *lagr-1(gk327);opls219* (to 0.9 ± 0.1 fold of control). These results indicate that mitochondrial ceramide contributes substantively to CED-4 displacement from mitochondrial membranes during radiation-induced germ cell apoptosis.

Our data indicate that the ceramide synthetic pathway is required for radiation-induced apoptosis of *C. elegans* germ cells. The most parsimonious molecular ordering suggests that CS (as well as its enzymatic product ceramide) functions on a pathway that is parallel to the CEP-1/p53–EGL-1 system. The coordinated function of these two pathways occurs at the mitochondrial commitment step of the apoptotic process. We hypothesize that ceramide may recompartmentalize the mitochondrial outer membrane, yielding a permissive microenvironment for EGL-1–mediated displacement of CED-4, the trigger for the effector stage of the apoptotic process.

References and Notes

1. E. Gulbins, P. L. Li, *Am. J. Physiol. Regul. Integr. Comp. Physiol.* **290**, R11 (2006).
2. K. Hofmann, V. M. Dixit, *Trends Biochem. Sci.* **23**, 374 (1998).
3. F. M. Goni, A. Alonso, *Biochim. Biophys. Acta* **1758**, 1902 (2006).
4. Materials and methods are available as supporting material on *Science* Online.
5. A. Gartner, S. Milstein, S. Ahmed, J. Hodgkin, M. O. Hengartner, *Mol. Cell* **5**, 435 (2000).
6. E. R. Hofmann *et al.*, *Curr. Biol.* **12**, 1908 (2002).
7. L. Geeraert, G. P. Mannaerts, P. P. van Veldhoven, *Biochem. J.* **327**, 125 (1997).
8. S. Spassieva *et al.*, *J. Biol. Chem.* **281**, 33931 (2006).
9. That *hyl-1* and *hyl-2* encode ceramide syntheses is clearly shown by their ability to restore growth to nearly

WT levels when expressed in Lag1/Lac1 double yeast mutants (*10*).
10. J.-C. Martinou, H. Riezman, personal communication.
11. Y. Pewzner-Jung, S. Ben-Dor, A. H. Futerman, *J. Biol. Chem.* **281**, 25001 (2006).
12. A small amount of C16:0:0 ceramide with a C17 sphingosine base (2% of the amount of the most abundant species C22:0:1) can be detected in *C. elegans* extracts (*13*).
13. H. Riezman, personal communication.
14. T. A. Taha *et al.*, *FASEB J.* **20**, 482 (2006).
15. X. Deng *et al.*, *Nat. Genet.* **36**, 906 (2004).
16. B. Schumacher *et al.*, *Cell Death Differ.* **12**, 153 (2005).
17. J. S. Duerr, in *Worm Book* (The *C. elegans* Research Community, WormBook, 2007), www.wormbook.org.
18. A. M. Labrousse, M. D. Zappaterra, D. A. Rube, A. M. van der Bliek, *Mol. Cell* **4**, 815 (1999).
19. K. De Vos *et al.*, *J. Biol. Chem.* **273**, 9673 (1998).
20. L. del Peso, V. M. Gonzalez, N. Inohara, R. E. Ellis, G. Nunez, *J. Biol. Chem.* **275**, 27205 (2000).
21. B. Conradt, H. R. Horvitz, *Cell* **93**, 519 (1998).
22. W. D. Fairlie *et al.*, *Cell Death Differ.* **13**, 426 (2006).
23. F. Chen *et al.*, *Science* **287**, 1485 (2000).
24. N. Yan *et al.*, *Mol. Cell* **15**, 999 (2004).
25. Y. Zermati *et al.*, *Mol. Cell* **28**, 624 (2007).
26. We thank Caenorhabditis Genetics Center and National BioResource Project-Japan for the strains provided; H. R. Horwitz for the anti–CED-4 antibody; Y. Gruenbaum for the anti–Ce-lamin-antibody; M. O. Hengartner for the strain opls219; and S. Davidor, D. Chau, H. Lee, J. Mesicek, and the Molecular Cytology and Genomics Core Laboratory of MSKCC for the technical assistance. This work was supported by grants CA85704 (R.K.), CA105125-03 (A.H.-F.), and 2R01HD42680-06 (S.S.).

Supporting Online Material
www.sciencemag.org/cgi/content/full/322/5898/110/DC1
Materials and Methods
Figs. S1 to S5
Tables S1 to S3
References

20 March 2008; accepted 9 September 2008
10.1126/science.1158111

Lacking Control Increases Illusory Pattern Perception

Jennifer A. Whitson[1]* and Adam D. Galinsky[2]

We present six experiments that tested whether lacking control increases illusory pattern perception, which we define as the identification of a coherent and meaningful interrelationship among a set of random or unrelated stimuli. Participants who lacked control were more likely to perceive a variety of illusory patterns, including seeing images in noise, forming illusory correlations in stock market information, perceiving conspiracies, and developing superstitions. Additionally, we demonstrated that increased pattern perception has a motivational basis by measuring the need for structure directly and showing that the causal link between lack of control and illusory pattern perception is reduced by affirming the self. Although these many disparate forms of pattern perception are typically discussed as separate phenomena, the current results suggest that there is a common motive underlying them.

The desire to combat uncertainty and maintain control has long been considered a primary and fundamental motivating force in human life (*1*–*3*) and one of the most important variables governing psychological well-being and physical health (*4*–*6*). For example, when individuals can control, or even just perceive that they can control, the duration of painful shocks, they show lower arousal (*7*); similarly, learning details about a painful medical procedure can reduce anxiety and even lead to shorter recovery time (*8*). In contrast, lacking control is an unsettling and aversive state, activating the amygdala, which indicates a fear response (*9*). It is not surprising, then, that individuals actively try to reestablish control when it disappears or is taken away (*10*).

We propose that when individuals are unable to gain a sense of control objectively, they will try to gain it perceptually. Faced with a lack of control, people will turn to pattern perception, the identification of a coherent and meaningful interrelationship among a set of stimuli. Through pattern perception, individuals can make sense of events and develop predictions for the future (*11*–*13*). For instance, spontaneous causal attributions (identifying a cause-and-effect pattern in a sequence of events) are best predicted by unexpected events rather than negative ones, suggesting that a major determinant of sense-making behavior is whether an individual lacks control (*14*, *15*). Indeed, researchers have designated "desire for control as a motivational force behind the attribution process" (*16*).

Related to our theoretical framework, research has found that current needs can shape and even bias perceptual processes. For example, children of lower economic status overestimate the size of coins as compared with the wealthy (*17*), and hungry individuals are more likely to see food in ambiguous images (*18*). This research has established that specific needs alter the perception of stimuli directly relevant to those needs. The current research explores a much broader phenomenon: whether lacking control creates a tendency to see patterns more generally.

Because these feelings of control are so essential for psychological well-being, our main hypothesis is that lacking control will lead to illusory pattern perception, which we define as the identification of a coherent and meaningful interrelationship among a set of random or unrelated stimuli (such as the tendency to perceive false correlations, see imaginary figures, form superstitious rituals, and embrace conspiracy beliefs, among others). In fact, a high desire for control has been associated with distortions of objective reality (*19*), and studies have found that lacking control produces attributional biases to restore feelings of control (*16*). We suggest that a lack of control provokes seeing and seeking patterns because pattern perception is a compensatory mechanism designed to restore feelings of control. Conspiracy beliefs are one example of how this process might work: They have been described as giving "causes and motives to events that are more rationally seen as accidents . . . [in order to] bring the disturbing vagaries of reality under . . . control" (*20*).

There are a number of findings that circumstantially support our specific hypothesis that lacking control leads to illusory pattern perception. Such disparate groups as preindustrial fisherman, skydivers, baseball players, and first-year MBA students have all displayed a connection between a lack of control and perceiving illusory patterns in one's environment. Tribes of the Trobriand islands who fish in the deep sea, where sudden storms and unmapped waters are constant concerns, have far more rituals associated with fishing than do those who fish in shallow waters (*21*). Parachute jumpers are more likely to see a nonexistent figure in a picture of visual noise just before a jump than at an earlier time (*22*). Baseball players create rituals in direct proportion to the capriciousness of their position (for example, pitchers are particularly likely to see connections between the shirt they wear and success) (*23*). First-year MBA students are more susceptible to conspiratorial perceptions than are second-year students (*24*). Even on a national level, when times are economically uncertain, superstitions increase (*25*). These anthropological observations and correlational studies all provide suggestive but nonconclusive evidence that lacking control leads to the perception of illusory patterns.

To test whether a lack of control directly increases illusory pattern perception, we conducted six experiments that used multiple methods to induce a lack of control and measured illusory pattern perception by using a variety of stimuli. Our definition of pattern perception, both illusory and accurate, encompasses a range of phenomena that were previously studied independently. Despite their surface disparities, seeing figures in noise, forming illusory correlations, creating superstitious rituals, and perceiving conspiracy beliefs all represent the same underlying process: the identification of a coherent and meaningful interrelationship among a set of random or unrelated stimuli.

In the first experiment, we sought to establish that lacking control creates a need to see patterns. We manipulated lack of control by using a concept-identification paradigm specifically created to re-

[1]Department of Management, The University of Texas at Austin, Austin, TX 78712, USA. [2]Department of Management and Organizations, Northwestern University, Evanston, IL 60208, USA.

*To whom correspondence should be addressed. E-mail: jennifer.whitson@mccombs.utexas.edu

Supporting Online Material for

Ceramide Biogenesis Is Required for Radiation-Induced Apoptosis in the Germ Line of *C. elegans*

Xinzhu Deng, Xianglei Yin, Richard Allan, Diane D. Lu, Carine W. Maurer, Adriana Haimovitz-Friedman, Zvi Fuks, Shai Shaham, Richard Kolesnick*

*To whom correspondence should be addressed. E-mail: r-kolesnick@ski.mskcc.org

Published 3 October 2008, *Science* **322**, 110 (2008)
DOI: 10.1126/science.1158111

This PDF file includes:

Supporting Online Material

Methods

Generation of mutant alleles in the ceramide pathway: Worms carrying homozygous deletion alleles *hyl-1(ok976), hyl-2(ok1766), lagr-1(gk327), lagr-1(gk331), sphk-1(ok1097), sptl-1(ok1693), sptl-3(ok1927)* and *T10B11.2(ok1252)* were isolated at the *C. elegans* Gene Knockout Consortium (Oklahoma). *tag-38(tm470), asm-3(tm2384)* and *T27F6.6(tm2178)* were isolated at the National Bioresource Project of Japan. *hyl-1(ok976), lagr-1(gk327)* and *tag-274(ok1097)* were backcrossed three times into the wild-type, and the deletion boundaries were determined by genomic DNA sequence analysis.

Nematode strains and strain construction: *C. elegans* worms were cultured as described by Brenner (*1*) at 20˚C. Wild-type N2, *egl-1(n1084n3082), ced-3(n717), ced-4(n1162), ced-9(n1950)* and *cep-1(gk138)* strains were provided by the Caenorhabditis Genetics Center. *abl-1(ok171)* was isolated as described previously (*2*). The CED-4::GFP line (*opIs219*) was provided by Dr. Michael Hengartner. Double mutants *lagr-1(gk327);hyl-1(ok976), hyl-1(ok976);abl-1(ok171)*, *lagr-1(gk327);abl-1(ok171), lagr-1(gk327);opIs219,* and *lagr-1(gk327);sphk-1 (ok1097),* and the triple mutants *lagr-1(gk327);hyl-1(ok976);abl-1(ok171)* and *lagr-1(gk327);hyl-1(ok976);ced-3(n717),* were generated and confirmed by single-worm polymerase chain reaction (PCR) as described (*2*).

Primers for strain isolation and identification:

	mutant allele (MT)	wild-type allele (WT)
hyl-1 (ok976)	5’-ccacgtcacttcgtacagag-3’	5’-ccacgtcacttcgtacagag-3’
	/5’-gccaaagaggaatatagaagg-3’	/5’-cttgttgtgagcatcatatcg-3’
lagr-1 (gk327)	5’-agatggacaaattaacggcg-3’	5’-acacacatgtggaagtagaat-3’
	/5’-gtcatggacccaacaacaca-3’	/5’- cattcccatcgtctatgatct-3’
sphk-1 (ok1097)	5’-ggcagttgatgagaaaacgg-3’	5’-ggcagttgatgagaaaacgg-3’
	/5’-gtgctttgcatatcgattttct-3’	/5’-gataatcagtcatatgcatcgt-3’
abl-1(ok171)	5’-atatgcctccctcctttgct-3’	5’-ttttgctttcaactcgcctt-3’

	/5'-ttttgctttcaactcgcctt-3'	/5'-gggaatctcttcattctcgg-3'
ced-3(n717)	5' -cggcttctttctccacacttgtta- 3'	/5' -cggcttctttctccacacttgcta- 3'
	5' -ggcgcacaccccatttgcattg- 3'	/5' -ggcgcacaccccatttgcattg- 3'

Phenotypic analysis of mutant animals: To measure somatic cell death, extra cells in the anterior pharynx were counted in larvae at L3 and L4 stages of development as previously described (*3*). Adult hermaphrodite germ cell nuclei were stained with DAPI and counted manually from 3-dimensional images acquired at 20X magnification. Reproductive/behavioral studies (embryo survival, male mating efficiency, and brood size) in wild-type, *hyl-1(ok976), lagr-1(gk327),* and the double mutant *lagr-1(gk327);hyl-1(ok976)* were performed as described in (*4*). Rates of germ cell corpse removal were determined as described previously (*2*). Significant differences were not detected between wild-type, and *hyl-1(ok976)* and *lagr-1(gk327)* worms with respect to gonad size, number of germ cell nuclei or brood size, excluding the possibility that gonadal developmental defects might have affected corpse number (Table S2). Germ cell apoptosis, induced by exposure to IR produced by a radioactive Cs^{137} source, was identified as in (*5*) and confirmed with SYTO 12 staining. Imaging was performed with a Zeiss Axioplan 2 microscope equipped with Nomarski optics and standard epifluorescence filters.

C_{16}-ceramide on germ cell apoptosis: Fresh stock solution of 5 mM C_{16}-ceramide (Biomol) was prepared by dissolving desiccated C_{16}-ceramide in ethanol containing 2% dodecane (vehicle) at 37°C. To induce germ cell apoptosis, the stock solution was diluted in M9 buffer (22 mM KH_2PO_4, 42 mM $NaHPO_4$, 85.6 mM NaCl, 1 mM $MgSO_4$) to the desired concentration and microinjected into the posterior gonad of young adult hermaphrodites. Controls received vehicle ($1x10^{-5}$-$5x10^{-2}$ dilution in M9 buffer). Germ cell corpses in the posterior gonad were counted at the indicated times after injection. For restoration of radiation-induced germ cell apoptosis, worms were irradiated immediately following ceramide injection. For these studies, sub-lethal doses of C_{16}-ceramide were titrated against restoration of the radiation response; while 0.001 μM gonadal ceramide (calculated as below) was ineffective, complete restoration was achieved at 0.005 μM gonadal ceramide.

To calculate gonadal ceramide concentration, we performed 1190 microinjections into wild-type worms using borosilicate glass capillaries (World Precision Instruments, IB100F-4, inner capillary diameter 0.58 μm). The microinjection capillary was mounted onto a Narishige MMN-1 coarse manipulator and connected to an Eppendorf Transjector 5246 (injection pressure: 1176hPa, compensation pressure: 276hPa, and injection duration: 0.4s). Images were taken of the fluid meniscus in the glass capillary before and after microinjection at 10X using a QIMAGING RETIGA 2000R FAST Mono Cooled Digital CCD Camera mounted onto an Axiovert S100 inverted microscope (Zeiss). Using QCapture Pro software to measure fluid displacement, we calculated each microinjection volume to be ~0.1 nL. Based on data from Brenner (*1*) that the dimensions of the adult hermaphrodite approximate a 1.0 mm x 0.08 mm cylinder, the volume of the entire adult was calculated as ~5.0 nL and of one gonadal arm as ~1.0 nL. Using this value and an injection volume of 0.1 nL, the gonadal ceramide concentration was calculated after C_{16}-ceramide microinjection.

Northern blot: Total and polyA-enriched RNA were isolated from wild-type and *hyl-1(ok976), lagr-1(gk327)* and *sphk-1(ok1097)* worms using the RNeasy kit (QIAGEN) and the MicroPoly(A)Purist mRNA purification kit, respectively (Ambion). The template DNA with T7 promoter was generated by PCR from cDNA of wild-type, *hyl-1(ok976), lagr-1(gk327)* and *sphk-1(ok1097)*. The anti-sense RNA probes were generated using T7 polymerases. Probes were labeled with [α-^{32}P]UTP using Strip-EZ RNA kit (Ambion) according to the manufacturer's instructions.

Quantitative RT-PCR: Synchronized wild-type, *hyl-1(ok976)* and *lagr-1(gk327)* hermaphrodites were irradiated with 120Gy at the young adult stage. Worms were collected at 0, 3 and 9 hours after radiation and total RNA was extracted using RNeasy Kit (QIAGEN) according to the manufacturer's instructions. 1 μg of total RNA was reverse-transcribed using the Thermoscript RT-PCR system (Invitrogen) at 52°C for 1 hour. 20 ng of resultant was used in a Q-PCR reaction using iCycler (Biorad) and the TaqMan Assay System for *egl-1* (probe: 5' AGCCGATCTCGTAGCCGATGCTGCT 3'; primer pairs: 5'CATGTTCTACTCCTCGTCTCAGG 3'/5'GTCAT CGCACATTGCTGCTAG 3'), and the control standard *mec-7* (probe: 5' AGCAGAAGCAATCAGCAGTATCGTGCCAT 3'; primer

pairs: 5'CTTCTTCATGCCAGGATTCGC 3'/5'GTCAACCTCCTTCATGCTCATTC 3'). *ced-13* expression was evaluated in a SYBR Green reaction as described by Schumacher et al. (*6*). The expression level of each sample was normalized to a control standard. For studying C_{16}-ceramide effects on *egl-1* and *ced-13* transcription, young adult worms were soaked in C_{16}-ceramide for 6 hours, transferred to seeded NGM plates, and RNA isolated 5 hours after recovery.

Ceramide quantification and mitochondrial colocalization by confocal microscopy: Freeze-cracking and immunostaining of dissected gonads were carried out according to WormBook (*7*) with minor modifications. Staining was performed on poly-L-lysine coated slides. Gonads were fixed in 4% formaldehyde (Ted Pella) in 0.1M phosphate buffer for 1 h on ice. After fixation, slides were incubated in antibody solution (PBS containing 0.1% BSA, 0.5% Triton X-100, 1mM EDTA and 0.05% sodium azide) for 5 min on ice, then in block solution (antibody solution containing 2% BSA) for 2 h at room temperature, washed twice with PBS and incubated for 30 min with PBSB (PBS containing 0.5% BSA). Thereafter, gonads were stained overnight at 4°C with anti-ceramide mouse monoclonal IgM antibody [MID15B4, Alexis Biochemicals diluted 1:30 (v/v)] in antibody solution, followed by Cy-3 anti-mouse IgM secondary antibody (1:200 dilution) for 1 hour at room temperature. While there is one report that MID15B4 is not specific for ceramide as measured by dot blot (*8*), we have performed both immune thin layer chromatography and an ELISA assay and find a high level of specificity as it does not detect other sphingolipids including the ceramide precursor dihydroceramide (Yin and Kolesnick, unpublished). For evaluation of mitochondrial ceramide, Alexa Fluor 488 conjugated monoclonal mouse IgG anti-human OxPhos Complex IV subunit 1 (Invitrogen) antibody at a 1:180 dilution was co-incubated with primary ceramide antibody, and co-localization detected using a Leica TCS SP AOBS scanning confocal microscope (63x objective, 2.5x digital zoom) at the same instrument settings for each sample. A region containing >20 cells just distal to the loop was selected for evaluation of ceramide intensity. Average pixel intensity over the region was calculated with Volocity 4.1 software.

CED-4 translocation in germ line by confocal microscopy: For immunostaining, germ cells were released from dissected gonads by gently pressing the coverslip before freeze-cracking.

Germ cells were first stained with anti-CED-4 antibody (provided by Dr. Robert Horvitz) at a 1:15 dilution in PBSB at 4°C overnight, and then stained with an FITC-conjugated secondary antibody (ZYMED Laboratories Inc.) for 1 hour at room temperature. Germ cells were subsequently incubated with anti-Ce-lamin antibody (1:100 dilution) (provided by Dr. Yosef Gruenbaum) for 1 hour followed by a 1-hour incubation at room temperature with secondary antibody (Alexa Fluor 594 goat anti-rabbit IgG, Invitrogen). CED-4 and lamin staining were viewed using a Zeiss fluorescence microscope, and fields of interest were identified and images acquired using a Leica TCS SP AOBS scanning confocal microscope (100x objective, 4x digital zoom) at the same instrument settings for each sample. Quantitation of fluorescence intensity at the germ cell nuclear membrane was performed using Metamorph software (version 7). Specificity of the anti-CED-4 antibody was confirmed using *ced-4(n1162)* worms that lack CED-4 (Fig. S5). To visualize CED-4 and mitochondria co-localization in live worms, *opls219* L1 larvae were placed on NGM (Nematode Growth Medium) agar plates containing 1 μg/ml Rhodamine B (Invitrogen) allowing mitochondria staining. The young adult worms were treated with 120Gy and the distribution of GFP (CED-4) and Rhodamine B (mitochondria) was imaged at 36 hours post-irradiation. We acquired z-stack images (63x objective, 2x digital zoom) at 1 micron intervals over an area containing one-third of the length of the distal arm adjacent to the gonadal loop. Colocalization of CED-4 and mitochondria was calculated with Metamorph software (version 7).

Statistics: Statistical differences between groups were calculated by Student's two-tailed *t* test.

Gene Product (s)	*C. elegans* Gene	WormBase Protein ID	Human ortholog		Mouse ortholog	
			Uniprot Accession Number	Identity	Uniprot Accession Number	Identity
Serine palmitoyltransferase 1	*sptl-1*	CE37749	O15269	50.7	O35704	51.6
Serine palmitoyltransferase 2	*sptl-3*	CE31996	O15270	48.6	P97363	48.6
Ceramide synthase	*hyl-1*	CE27675	Q96G23	32.7	Q924Z4	33.3
	hyl-2	CE34329	Q9HA82	29.3	Q9D6J1	29.9
	lagr-1	CE20184	P27544	30.0	P27545	29.4
Acid ceramidase	F27E5.1	CE01562	Q13510	34.2	Q9WV54	33.5
Sphingosine kinase	*sphk-1*	CE35833	Q9NYA1	29.6	O88886	30.2
Sphingosine phosphate lyase 1	*spl-1*	CE20348	O95470	37.8	Q8R0X7	38.3
	tag-38	CE06695	O96470	38.5	Q8R0X7	39.1
Ceramide kinase	T10B11.2	CE18241	Q8TCT0	25.8	Q8R0Q7	26.6
Acid sphingomyelinase	*asm-1*	CE30230	P17405	32.8	Q04519	32.0
	asm-2	CE31674	P17405	32.6	Q04519	34.3
	asm-3	CE39794	P17405	35.4	Q04519	35.5
Neutral sphingomyelinase	T27F6.6	CE34214	O60906	36.3	O70572	36.8

Table S1. Sequence comparison of proteins in the ceramide metabolic pathway.

Alignments for each class were performed using the ClustalW algorithm.

Table S2. Reproductive/behavioral control studies

	wild-type	*hyl-1(ok976)*	*lagr-1(gk327)*
Rate of germ cell corpse removal (min) ± SEM	31.2 ± 4.5 (10)	34.5 ± 2.8 (10)	40.6 ± 5.5 (9)
Germ cell nuclei ± SEM*	366.6 ±14.6 (10)	327.5 ±15.9 (10)	325.2 ±17.4 (10)
% Embryo survival ± SEM	97.5 ±4.2 (1019)	95.5 ±3.8 (1010)	95.8 ±4.0 (1259)
% Mating efficiency†	91.0	89.5	75.5
Brood size ± SEM	227.8 ±7.7 (22)	209.4 ±10.9 (20)	225.0 ±8.1 (25)

Data are presented as mean±SEM. (n) = number of animals. *The number of DAPI stained nuclei in one side of the distal gonad. †Assays for mating efficiency were performed in duplicate (*9*). For each strain, 16 males were mated with 16 late L4 stage *unc-51* hermaphrodites for 24 hours and then scored for cross progeny (non-*Dpy* progeny) and self progeny. Mating efficiency = cross progeny/total progeny.

Table S3. Loss-of-function mutations of ceramide synthases do not affect somatic cell death.

Genotype	Extra cells in the pharynx (n)
wild-type	0.05 ± 0.22 (20)
ced-3(n717)	12.1 ± 1.1 (15)
lagr-1(gk327)	0.1 ± 0.4 (30)
hyl-1(ok976)	0.17 ± 0.38 (30)
lagr-1(gk327); hyl-1(ok976)	0.07 ± 0.25 (30)
hyl-2 (ok1766)	0.25 ± 0.48 (57)

Extra cells in the anterior pharynx were counted in L3-L4 larvae. The apoptosis-defective *ced-3(n717)* was used as a positive control. Data are presented as mean±SD. (n) = number of animals.

Fig. S1A.

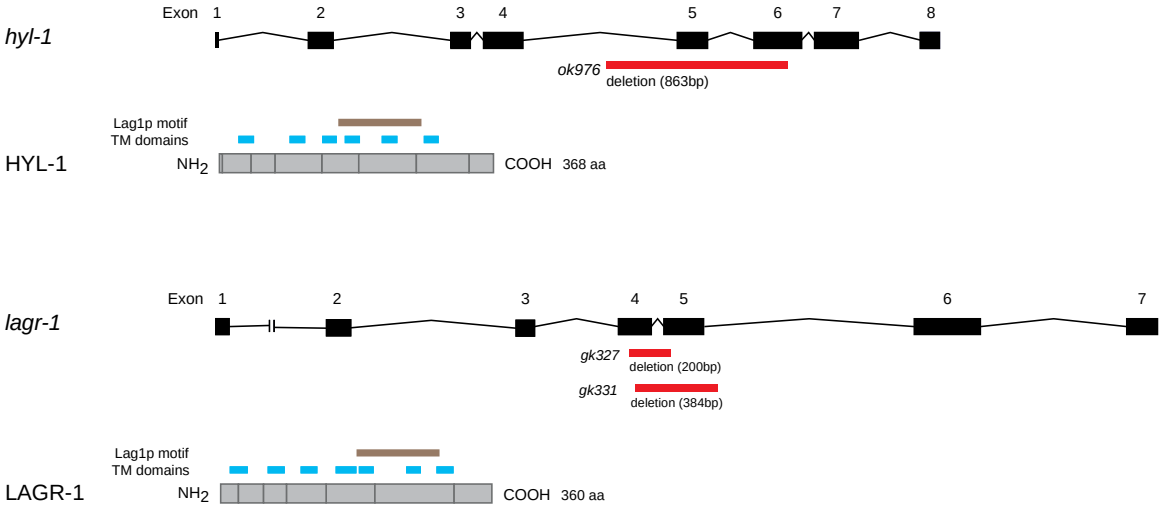

Fig. S1B.

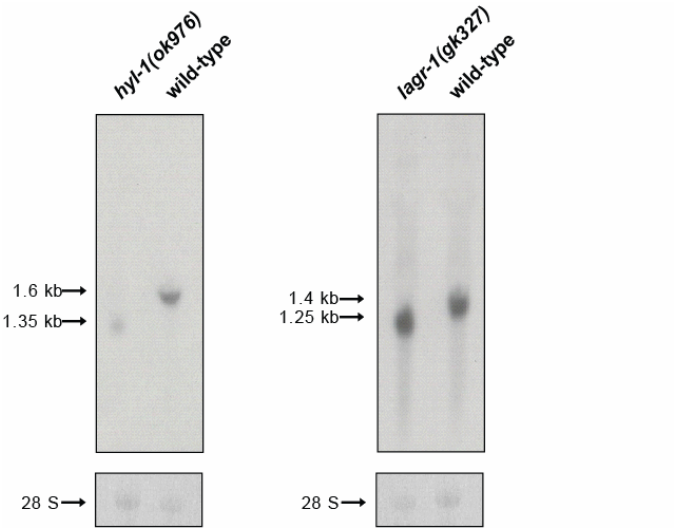

Figure S1C.

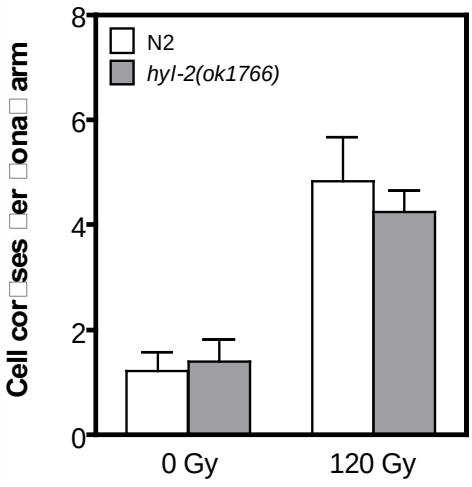

Fig. S1. Deletion alleles of *hyl-1(ok976), lagr-1(gk327)* and *hyl-2(ok1766)*. (**A**) Structure diagrams of *hyl-1* and *lagr-1*. Numbered boxes indicate exons, and introns are represented as lines. The genomic regions of each deletion are marked in red. In the diagram of HYL-1 and LAGR-1, transmembrane domains are marked in blue and Lag1p motifs are marked in brown. In *hyl-1(ok976)*, an 863 bp fragment from the *hyl-1* gene locus is deleted, eliminating exon 5 and 67% of exon 6, resulting in loss of the Lag1p coding sequence. In *lagr-1(gk327),* a 200 bp deletion from exon 4-5 corresponding to 150 bp of *lagr-1* cDNA results in a frame-shift that similarly disrupts the Lag1p motif. (**B**) Northern-blot analysis of *hyl-1(ok976)* and *lagr-1(gk327).* Northern blotting was performed using 3 μg of poly(A)-enriched RNA which were hybridized with RNA transcripts corresponding to cDNA bps 5-480 for *hyl-1* and bps 1-260 for *lagr-1*. 28 S rRNA was used as a loading control. In wild-type worms, a ~1.6 kb *hyl-1* transcript and a ~1.4 kb *lagr-1* transcript were detected, whereas a smaller ~1.35 kb transcript was observed in *hyl-1(ok976)* and a ~1.25 kb transcript in *lagr-1(gk327)*. (**C**) Germ cell corpses in *hyl-2(ok1766)* after 120Gy. Data (mean±SEM) are collated from 10-15 worms/group.

Fig. S2A.

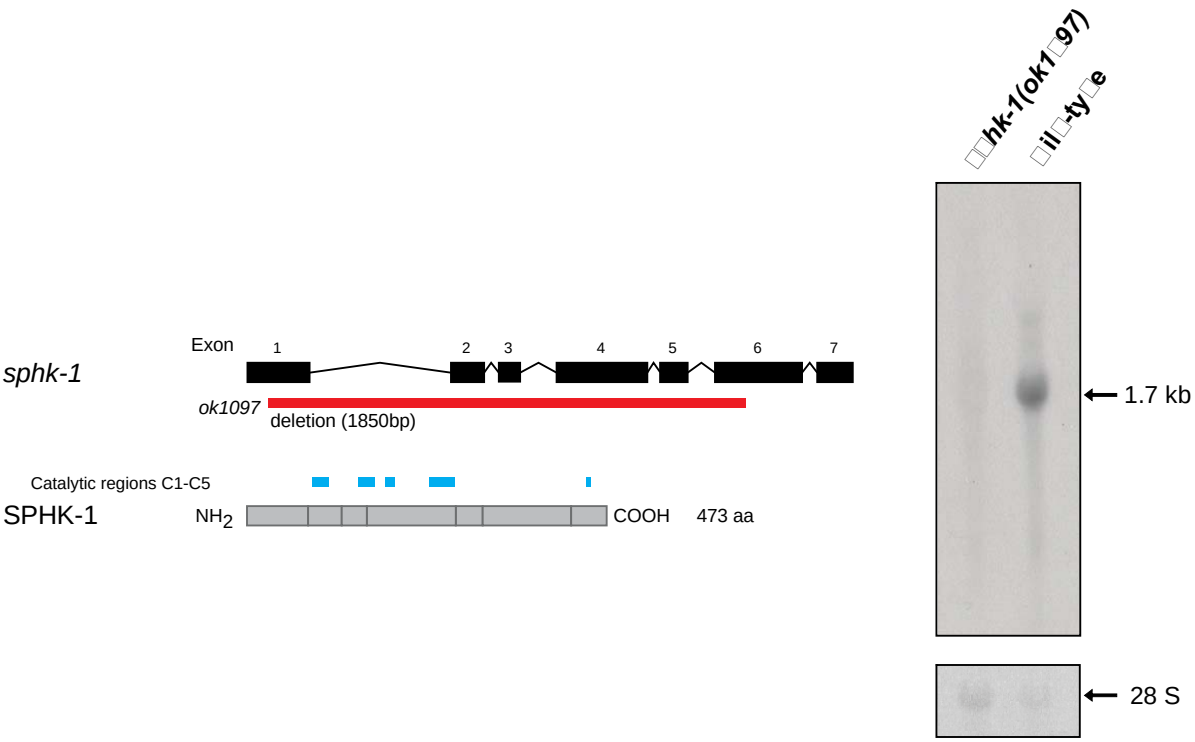

Fig. S2B.

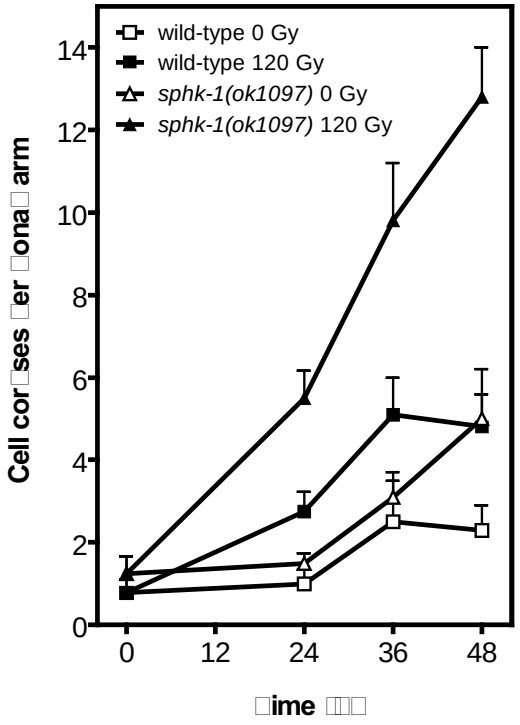

Fig. S2. *C. elegans* sphingosine kinase (SPHK) deletion allele *sphk-1(ok1097).* (**A**) *sphk-1* contains 7 exons. Four alternative splice variants of *C. elegans sphk* have been reported in Wormbase. *sphk-1* C34C6.5a is 1422 bp in length and *sphk-1* C34C6.5b1, b2 and b3 are 1272 bp in length with a shorter exon 1 (150bp). The region of deletion is marked in red. The catalytic regions of SPHK-1 are marked in blue. Northern blot analysis was performed using 3 µg of poly(A)-enriched RNA from wild-type and *sphk-1 (ok1097).* The blots were hybridized to an mRNA probe corresponding to bps 3-262 of *sphk-1* C34C6.5a coding sequence. 28 S rRNA was used as a loading control. While the wild-type SphK gene manifests a 1.7 kb transcript by northern blot analysis, *sphk-1(gk274)* manifests a 1.8 kb deletion from the gene locus corresponding to *sphk-1* exons 2-7, and displays no transcript. (**B**) Germ cell corpses in *sphk-1 (ok1097)* after 120Gy. Data (mean±SEM) are collated from 10-15 worms/group.

Fig. S3.

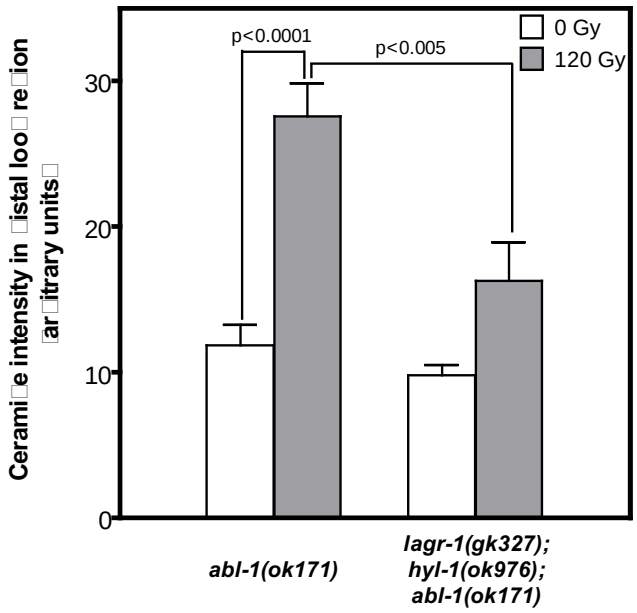

Fig. S3. Radiation-induced ceramide increase is abrogated in a CS mutant background. Gonads were dissected from young adult *abl-1(ok171)* and *lagr-1(gk327);hyl-1(ok976);abl-1(ok171)* at 24 hours after 120Gy and stained with anti-COX-IV antibody, anti-ceramide antibody and DAPI as in Fig. 3A. Gonadal ceramide intensity was quantified using Metamorph software. Data (mean±SEM) are from ≥14 gonads/group.

Fig. S4.

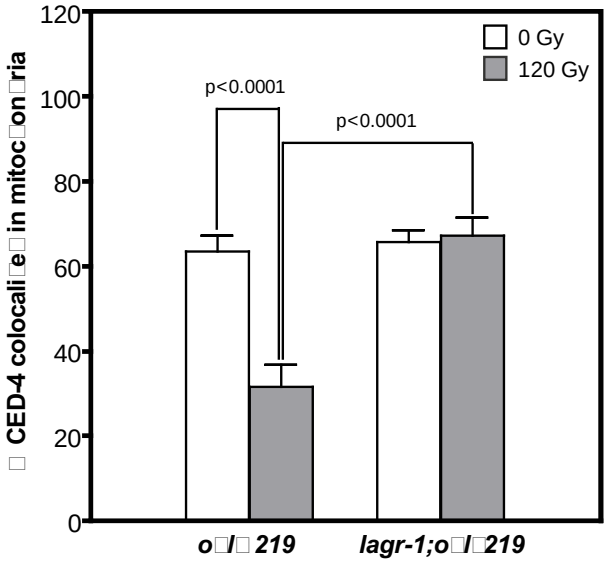

Fig. S4. *C. elegans* CS mutations block radiation-induced CED-4 reduction in mitochondria. L1 larvae of *opls219* and *lagr-1(gk327);opls219* were cultured on Rhodamine B-containing agar plates to the young adult stage, and then exposed to 120Gy. ~5 serials Z-stack images from each animal were evaluated for co-localization of CED-4 and mitochondria. Data (mean±SEM) are collated from ≥8 worms/group.

Fig. S5.

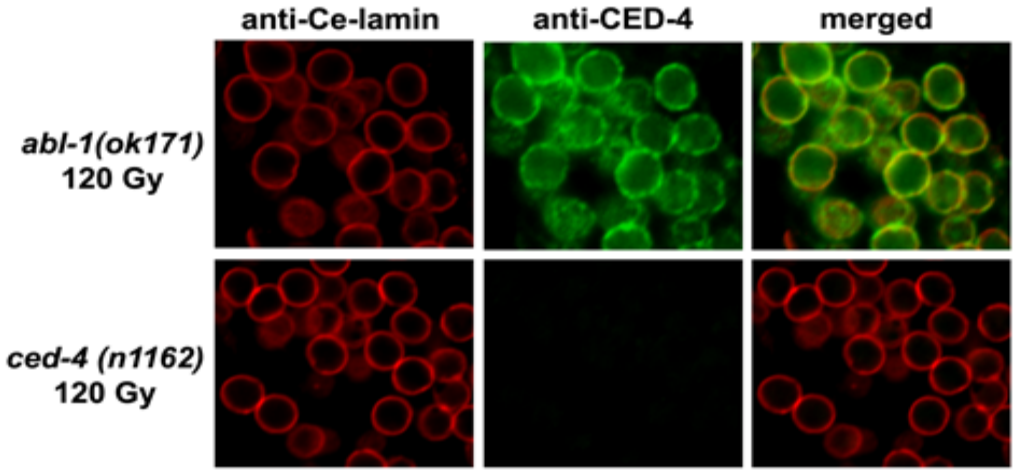

Fig. S5. Germ cells were released from gonads of young adult *abl-1(ok171)* and *ced-4(n1162)* at 24 hours after 120Gy, and stained with anti-Ce-lamin (red) and anti-CED-4 (green) as in Methods. CED-4 localizes to nuclear membranes in *abl-1(ok171*), but is absent in *ced-4(n1162)*.

Supporting Online References

S1. S. Brenner, *Genetics* **77**, 71 (1974).

S2. X. Deng *et al.*, *Nat Genet* **36**, 906 (2004).

S3. M. O. Hengartner, R. E. Ellis, H. R. Horvitz, *Nature* **356**, 494 (1992).

S4. J. M. K. Erik M. Jorgensen, in *worm book*. (The *C. elegans* Research Community / WormBook, 2007).

S5. T. L. Gumienny, E. Lambie, E. Hartwieg, H. R. Horvitz, M. O. Hengartner, *Development* **126**, 1011 (1999).

S6. B. Schumacher *et al.*, *Cell Death Differ* **12**, 153 (2005).

S7. J. S. Duerr, in *worm book*. (The *C. elegans* Research Community / WormBook,, 2007).

S8. L. A. Cowart, Z. Szulc, A. Bielawska, Y. A. Hannun, *J Lipid Res* **43**, 2042 (2002).

S9. J. Hodgkin, *Genetics* **103**, 43 (1983).